Advances in
Bridge Engineering

ORIGINAL INNOVATION Open Access

Fatigue performance of ECC link slab incorporated full RC girder joint-free bridges

Khandaker M. Anwar Hossain[1*], Katie Chu[1] and Mohamed Lachemi[1]

*Correspondence:
ahossain@torontomu.ca

[1] Dept. of Civil Engineering, Toronto Metropolitan University, Toronto, Canada

Abstract

The use of link slab (LS) made of Engineered Cementitious Composite (ECC) in the construction of joint-free bridge deck can meet structural performance requirements and enhance durability to minimize life cycle costs. Studies documented in the literature to date have been limited to composite steel-concrete I-deck girder bridges despite their commonly used reinforced concrete (RC) girder counterparts in construction. This paper deals with two span full RC deck girder joint-free bridges with ECC link slab (ECC-LS) constructed and tested under static and fatigue loading up to 1,000,000 cycles at 4 Hz subjected to mean stress level of 40% of girder ultimate load, followed by post-fatigue static loading to failure. Residual load, deflection, moment, rotation, stiffness, and energy absorbing capacity of fatigued bridge specimens are compared with its virgin (non-fatigued) counterparts to assess structural performance. Experimental moment capacities are compared with those obtained from existing analytical equations. The comparative performance of joint-fee bridge with RC deck girder is compared with its composite steel-concrete I-girder counterpart to assess its feasibility of construction.

Keywords: Joint-free bridge, Link slab, Engineered cementitious composite, Static and fatigue loading, Reinforced concrete deck girder, Residual strength

1 Introduction

Over the last decade, self-consolidating ECC has been developed with superior ductility and durability - which translates to speedy construction, reduced maintenance and a longer life span for the structure. Tensile strain capacity exceeding 5% has been demonstrated on ECC materials reinforced with polyethylene and polyvinyl alcohol fibres. ECC strain hardens after first cracking, and demonstrates a strain capacity 300 to 500 times greater than normal concrete. Even at large imposed deformation, crack widths of ECC remain small, less than 60 μm (Li 2003, 2019; Li and Li 2011; Zhang et al. 2019). Green and cost-effective ECC mixtures have been developed by incorporating industrial by-products and natural pozzolans as replacement of cement as well as locally available aggregates (Sahmaran et al. 2009; Sherir et al. 2018; Siad et al. 2018).

Viability of using ECC in infrastructure applications such as building and bridge structures has been investigated over the years (Caner and Zia 1998; Alampalli and Yannotti 1998; Kim et al. 2004; Lepech and Li 2009; Hossain et al. 2015; Chu et al.

Springer Open

© The Author(s) 2024. **Open Access** This article is licensed under a Creative Commons Attribution 4.0 International License, which permits use, sharing, adaptation, distribution and reproduction in any medium or format, as long as you give appropriate credit to the original author(s) and the source, provide a link to the Creative Commons licence, and indicate if changes were made. The images or other third party material in this article are included in the article's Creative Commons licence, unless indicated otherwise in a credit line to the material. If material is not included in the article's Creative Commons licence and your intended use is not permitted by statutory regulation or exceeds the permitted use, you will need to obtain permission directly from the copyright holder. To view a copy of this licence, visit http://creativecommons.org/licenses/by/4.0/.

2023). With intrinsically tight crack width and high tensile ductility, ECC represents a new generation of high-performance concrete material that offers significant potential to resolving the durability problem and increasing the service life of reinforced concrete (RC) structures (Hossain et al. 2020).

Deck joints represent one of the major sources of deterioration and typically require expensive maintenance or replacement over the service life of a bridge. Expansion joints can be replaced by flexible link slabs (which maintains rotational capacity of adjacent spans) forming a joint-free multi-span bridge and hence, solving the problem of premature corrosion deterioration components by not allowing deposition of moistures, chemicals and other debris (Caner and Zia 1998; Alampalli and Yannotti 1998; Li et al. 2003; Kim et al. 2004). The high strain capacity while maintaining low crack widths of ECC, make it an appropriate material for the link slab application. Figure 1 shows a typical two span joint-free bridge with a link slab (LS) showing expected moment diagram. LS is normally the part of the deck between inflection points and has debonding and transition zones. Testing on two-span joint-free steel and reinforced concrete (RC) girder bridges with conventional RC link slab (not ECC) exhibited the development of negative bending moment in link slab as shown in Fig. 1 (Caner and Zia 1998).

Research on isolated ECC link slab (ECC-LS) in composite deck-steel I- girder bridges under static and fatigue loading showed enhanced rotational capacity, microcracking characteristics, residual strength and energy absorbing capacity compared to their conventional concrete counterparts (Kim et al. 2004; Hossain et al. 2015; Chu et al. 2020, 2021; Zhang et al. 2021; Karim and Shafei 2021). The glass fiber reinforced polymer (GFRP) rebar incorporated LS exhibited better durability and rotational capacity compared to their steel rebar counterparts (Karim and Shafei 2021; Chu et al. 2020, 2021; Zhang et al. 2021). Experimental and numerical investigation on two span steel-concrete composite deck girder joint-free bridges with ECC link slab under static and fatigue loading also revealed satisfactory performance and viability of such construction (Chu et al. 2022a, 2023). ECC made or rehabilitated bridge and building elements also showed higher strength, ductility and durability compared to their

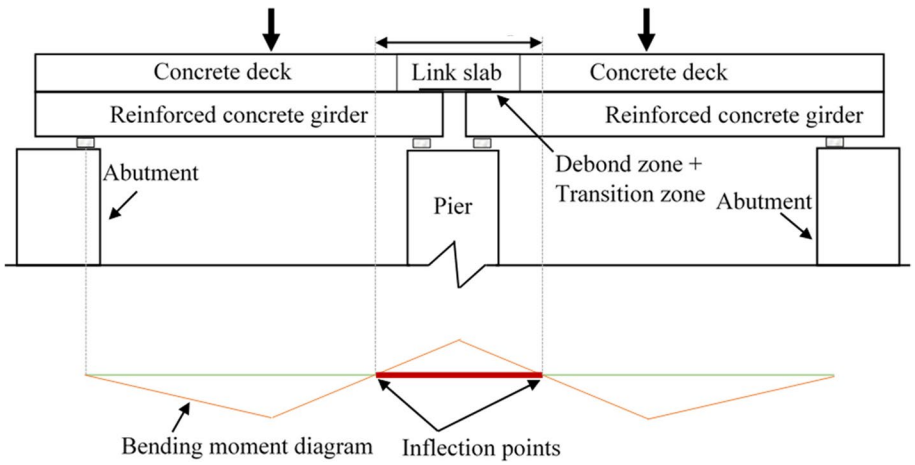

Fig. 1 Joint-free bridge with link slab

conventional concrete counterparts (Yeganeh and Hossain 2023; Hossain et al. 2019, 2020, 2021; Zhou, et al. 2021, Huang et al. 2021).

Notable amount of research has been conducted on ECC incorporated joint-free bridge and individual LS having steel-concrete composite I-girders. A study on individual ECC link slab incorporated in RC deck girder bridge was conducted recently (Chu et al. 2022b) with no research on LS incorporated full joint-free bridges till to-date. Hence investigation on full RC deck girder joint-free bridge is warranted to understand fully the structural behaviour as study on isolated ECC-LS could not provide sufficient information. The evaluation of structural performance of ECC-LS incorporated RC deck girder joint-free bridges is the novel aspect of this study. This paper presents test results of two-span pin-supported T-shape RC deck girder full joint-free bridges with ECC-LS subjected to static loading to failure and up to 1,000,000 fatigue load cycles at a chosen stress level before being loaded to failure under monotonic load. The pre-fatigue-fatigue/post-fatigue load-deflection or moment-rotation responses, strain development, cracking characteristics, failure modes and energy absorption capacities are analysed to compare performance with their counterparts similar steel-concrete composite -girder joint-free bridges from previous research studies (Chu et al. 2022a, 2023). Experimentally obtained load and moment capacities of RC-LS and joint-free bridge are also compared with those obtained from existing analytical models.

This study has made meaningful contributions in understanding static and fatigue behaviour of novel RC deck girder joint-free bridges with ECC-LS and formulating design guidelines that will benefit engineers, researchers and local authorities.

2 Experimental investigation

Two identical two-span pin-supported joint-free RC deck girder bridge specimens (designated as B0N and B4H) with ECC-LS were tested whose details are shown in Table 1. B0N was tested under monotonic loading to failure, while B4H was first subjected to fatigue loading at 40 ± 10% stress level for 1,000,000 cycles before being loaded to failure under monotonic loading failure in the post-fatigued stage. The designation 'B0N' (in Table 1) represents joint-free bridge (B) specimen tested under zero stress level (0) and no fatigue cycle (N) while 'B4H' represents joint-free bridge (B) specimen tested at 40% stress level (4) for 1,000,000 fatigue cycles (H).

The dimensions and steel reinforcement details in bridge specimens are shown in Fig. 2(a-b). The dimensions were chosen based on 1/12th scale of the bridge simulated by Caner and Zia (1998). Some modifications to deck thickness and debond zone length were needed to improve constructability of the small-scale specimens as used previously for steel-concrete composite I-deck- girder bridges (Chu et al. 2023). However, deck slab thickness-to-debond zone length ratio was maintained close to that used by Caner and Zia (1998). The bridge specimens had two adjacent RC slab on girder (T-girders) as main spans (each of 1150 mm in length) with an ECC-LS having 340 mm transition and 240 mm debond zones (Fig. 2a). Deck girders were composed of a concrete T-section reinforced with 4-10 M longitudinal steel bars in two layers in the web, and stirrups (6 mm diameter bars @ 39 mm c/c) extending into the flange or bridge deck (Fig. 2a-b). In steel-concrete composite I-deck- girder bridges, shear studs are used to connect steel girder to concrete deck. Stirrups were not extended

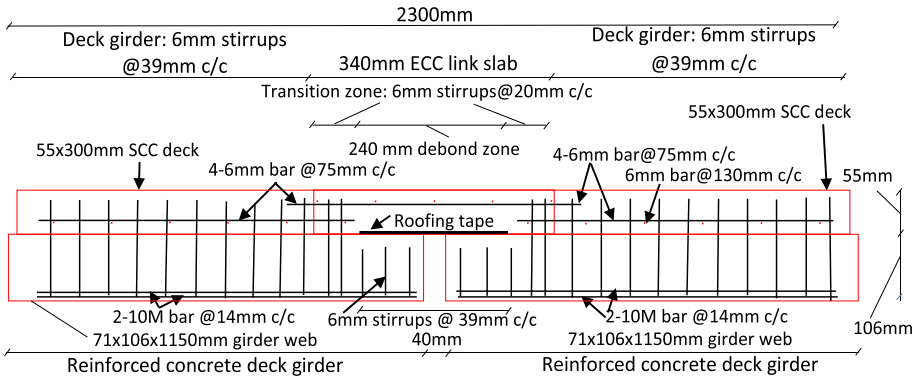

(a) Joint-free bridge specimen design details

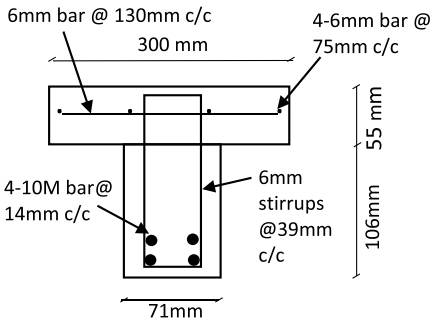

(b) Cross-section of T-deck girder

(c) Girder reinforcement and formwork

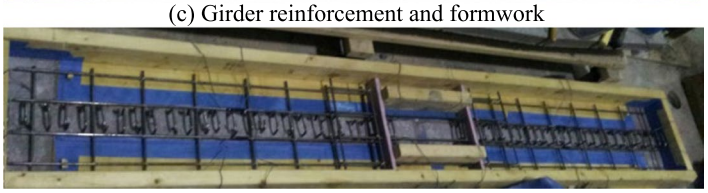

(d) deck reinforcement and formwork

Fig. 2 Joint-free bridge specimens: design and construction details. **a** Joint-free bridge specimen design details. **b** Cross-section of T-deck girder. **c** Girder reinforcement and formwork. **d** deck reinforcement and formwork

from the girder web to the link slab within the debond zone (which is typically 5% of span length) to improve link slab flexibility. In addition, smooth frictionless interface was ensured by placing roofing tape between deck and girder web. Kim et al. (2004) proposed link slab design details to include a transition zone extending on either side of the debond zone to transition between two materials from the ECC link slab to the normal concrete deck. The transition zone was introduced on either side of the ECC-LS to prevent premature failure at the interface between LS-ECC and main deck interface and this was achieved by doubling the amount of stirrups (6 mm bar @ 20 mm c/c) (Fig. 2a) in this zone. In the ECC-LS and bridge deck Sect. (300×55 mm)

Table 1 Specimen details, material properties, and testing regime

Geometric dimensions and material properties							
Designation	Specimen Type	Overall Length (mm)	Debond Zone Length (mm)	Transition Zone Length (mm)	Girder & Deck Material	Link Slab Material	Rebar Material
B0N	Full bridge	2300	240	340	SCC	ECC	Steel
B4H							
Testing scheme							
Designation	Loading Type			Number of Cycles	Mean Stress Level (%)		
B0N	Static monotonic			0	N/A		
B4H	Fatigue-post-fatigue monotonic			1,000,000	40±10		

Commercial SCC: Portland cement, silica fume, 10 mm aggregate and admixtures

ECC: mortar sand, Portland cement, class C fly ash, high-range water-reducing admixture, 10 mm-long polyvinyl alcohol fibres

Compressive strength: 51 MPa (SCC); 62 MPa (ECC); flexural strength is 5.8 MPa (SCC), 6.1 MPa (ECC), Steel yield strength = 400 MPa (Mean values of at least three specimens)

as shown in Fig. 2(a-b), minimum longitudinal reinforcing ratio of 0.01 (3–6 mm dia bars) and minimum transverse reinforcements for temperature and shrinkage (6 mm diameter bars at 210 mm c/c were provided as per existing design guidelines (Lepech and Li 2009; Chu et al. 2022b).

A commercial self-consolidating concrete (SCC) was used to cast first the bridge deck girder parts and after 24 h, middle link slab part was cast using an ECC. Figure 2(c-d) show reinforcements and formworks before casting of SCC/ECC to make bridge specimens. SCC and ECC mix details are presented in Table 1 and more details on mixing and casting procedures can be found in Chu et al. (2022b). The compressive and flexural strengths of SCC and ECC were determined using control cylinder (100×200 mm) and beam ($355 \times 75 \times 50$ mm) specimens. Joint-free bridge and control specimens were moist cured for 7 days at 23°C and then air cured in the laboratory until testing at the age of 28 days. Rebar properties were determined by testing coupon specimens. Properties of SCC, ECC and rebar materials are presented in Table 1.

3 Theoretical analysis

The moment capacity ($M_{r\text{-}g}$) of RC T-deck girder is determined based on Eq. 1 considering deck (flange) and web reinforcement using strain (€) and stress/force diagrams as shown in Fig. 3.

$$M_{r-g} = \varphi_s f_y A_s \left(d - \frac{a}{2}\right) = 15.85kNm \tag{1}$$

$$a = \frac{\varphi_s f_y A_s}{a_1 \varphi_c f_c' b_e} \tag{2}$$

where $\phi_s = (1.0)$: steel material reduction factor, f_y (=400 MPa) and A_s (=0.000412m^2) : rebar yield strength and area, respectively, d (= 0.103m) :effective depth, a (=0.013m): rectangular stress block depth from Eq. 2, α_1 (=0.8), ϕ_c (= 1.0) : concrete material

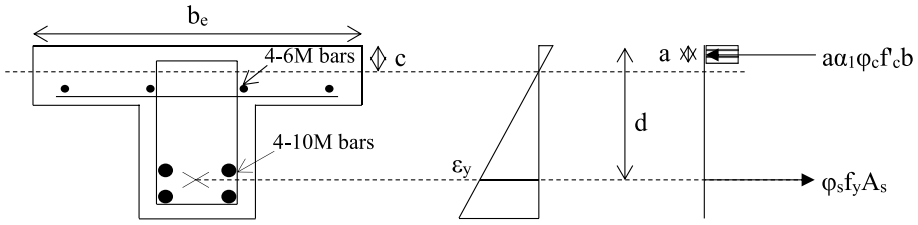

Fig. 3 RC deck girder analysis

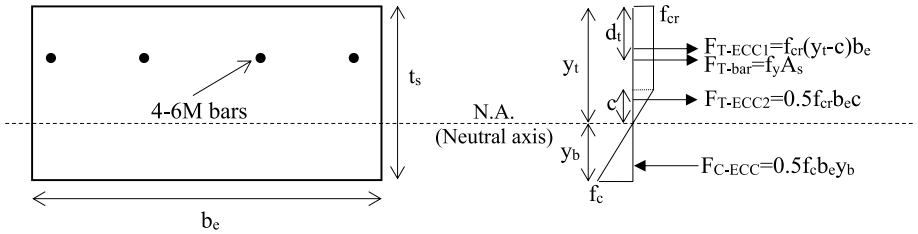

Fig. 4 ECC link slab analysis

reduction factor, f'_c (= 51 MPa): concrete compressive strength, and b_e (= 0.3 m): effective flange width.

ECC-LS resists bending moment due to adjacent girder end rotations as shown in Fig. 1 (Caner and Zia 1998). The moment capacity of ECC-LS (M_{r-LS}) is calculated using stress/force diagram (Fig. 4) taking into account ECC tensile force components F_{T-ECC1} ($=f_{cr}(y_t\text{-}c)b_e$) and F_{T-ECC2} ($=0.5f_{cr}b_ec$) as per Li et al. (2003) as well as rebar tensile force F_{T-bar} ($=f_yA_s$) and ECC compressive F_{C-ECC} ($=0.5f_cb_ey_b$) using Eq. 3 (Lepech and Li 2009).

$$M_{r-LS} = F_{T-ECC1}\left(\frac{y_t - c}{2} + c\right) + F_{T-ECC2}\frac{2}{3}c + F_T - bar\left(y_t - d_t\right) + F_{c-ECC}\tfrac{2}{3}y_b = 2.01\ kNm \tag{3}$$

where c: depth of triangular stress block, b_e: effective width of the slab, t_s: total slab thickness, d_t: rebar distance from top, y_t and y_b: distance of neutral axis (N.A.) from top and bottom, respectively, f_{cr} (assumed to be 3.45 MPa as per Li et al. 2003) and f_c: ECC cracking strength under uniaxial tension and compressive strength, respectively. Detailed calculations can be found in Chu et al. (2022b).

4 Joint-Free bridges with RC Deck Girder

4.1 Experimental setup

The RC deck girder full joint-free bridge specimen B0N (non-fatigued) with ECC link slab (Table 1) was placed on four roller supports for static testing to failure using a loading system which applied load at a rate of 3 kN/min (Fig. 5a-b). The exterior rollers were shimmed to prevent horizontal movement. The bridge was loaded by a spreader beam such that a line load was applied in the middle of each of the adjacent spans to induce positive moment in the girders (Fig. 5a-b).

Table 2 Deflections of joint-free bridge at the start and end of fatigue cycles

Deflection	Girder	Link Slab
Start of cycles (mm)	-4.00	0.23
End of cycles (mm)	-4.66	0.33
Change in deflection (%)	17	42

- Downward + upward

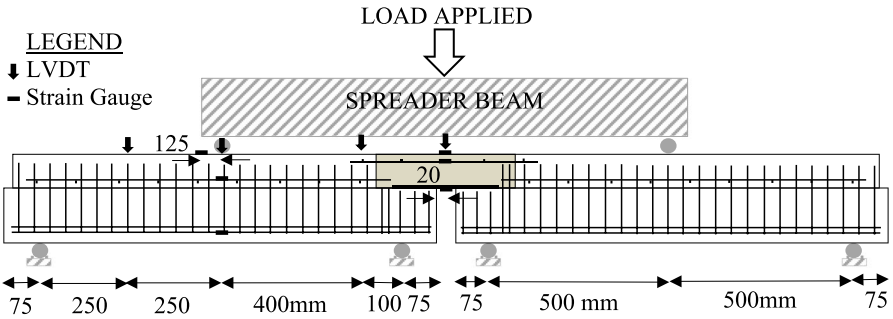

(a) Schematic of RC deck girder joint-free bridge loading with instrumentation

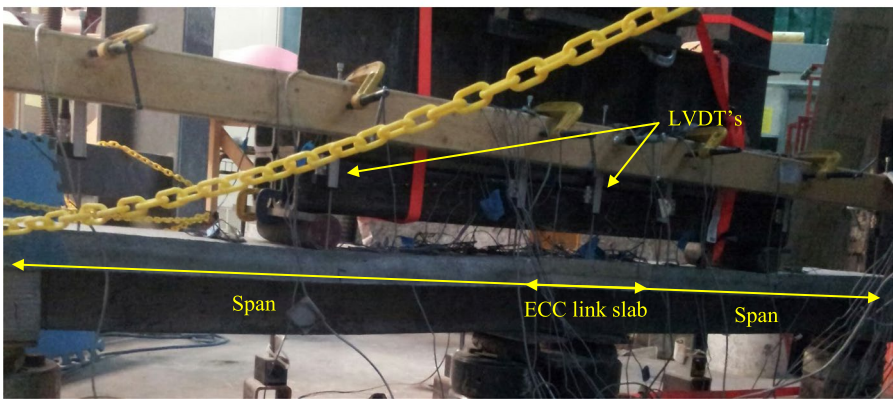

(b) Joint-free bridge test setup and instrumentation

Fig. 5 Testing and instrumentation of RC deck girder joint-free bridge. **a** Schematic of RC deck girder joint-free bridge loading with instrumentation. **b** Joint-free bridge test setup and instrumentation

RC deck girder joint-free bridge specimen B4H was subjected to fatigue loading using the same test setup as for monotonic loading (Fig. 5a-b). Initial ramp to fatigue was applied at 3 kN/min up to 40% of RC girder yield load of the virgin specimen B0N. Once the mean stress level was achieved, fatigue load was applied at $40 \pm 10\%$ stress level for up to 1,000,000 cycles (at 4 Hz). Fatigue load was stopped for minimum 2 h every 200,000 cycles to allow the hydraulic system to cool. After cumulative 1,000,000 cycles, the specimen was unloaded to 0 kN prior to initiating post-fatigue static load to failure using the same procedure as specimen B0N.

Load, displacement, and strain development were recorded at strategic locations (Fig. 5a-b) during the test using a computer aided data logger. Linear voltage displacement transducers (LVDTs) were used to record vertical displacements at various locations including midspan of girders and link slab to determine overall deflected shape of the bridge and calculate girder end rotations. The variation of strain across the link

slab depth at mid span was recorded using strain gauges installed at the top and bottom surfaces of the ECC-LS and embedded rebar. The strain variation at mid span of the bottom layer of rebar in RC girder strain was also recorded (Fig. 5a-b). Cracking, crack progression and failure modes were visually observed during testing. After unloading of the failed specimens, cracks were counted, and widths measured using a crackscope accurate to the nearest 0.05 mm.

4.2 Test results during fatigue loading and discussion

The fatigue behaviour of specimen B4H subjected to 1,000,000 cycles at $40 \pm 10\%$ fatigue stress level was assessed based on load-deflection response and strain development at both the bridge mid-span, and at the middle of the link slab. Results were compared with a companion steel girder joint-free bridge with ECC link slab which was also subjected to same fatigue stress level and number of cycles. The main difference between the reinforced concrete and steel girder bridges was in their flexural rigidity (EI), which was 7.9 times higher for the steel girder compared to its reinforced girder counterpart.

Load-deflection responses at girder mid-span (one of the two girders is shown due to symmetry) and middle of link slab of Specimen B4H during 1 million cycles of fatigue loading are shown in Fig. 6a. Deflections at both locations increased with the increase fatigue cycles, however RC deck girder downward (-ve value) mid-span deflection remained within 5 mm compared to 0.5 mm of link slab upward (+ve value) deflection throughout 1,000,000 cycles of fatigue loading. Table 2 presents deflections at the start and end of fatigue cycles, and corresponding deflection bandwidths calculated as the difference between the two values. Girder and link slab mid-span deflections increased by 17% and 42%, respectively as fatigue cycles progressed. These increases are greater than those observed in composite steel girder specimens (Chu et al. 2023) of similar dimensions and materials. Therefore, the reinforced concrete girder specimen showed improved main bridge span flexibility due to lower EI. Flexibility of the reinforced concrete girder also allowed for higher increase in link slab deflection compared to its steel girder counterpart. In contrast, high EI of the steel girders limited bridge mid-span deflection and corresponding link slab deflection increase during fatigue loading.

Figure 6b shows that instantaneous stiffness (calculated as load per span divided by corresponding mid-span deflection from load-deflection response) of the joint-free RC bridge deck girder decreased by 12% (from 7.65 kN/mm to 6.73 kN/mm) after 1,000,000 fatigue cycles and exhibited more degradation than its composite steel deck girder counterpart (Chu et al. 2023) due to crack development and propagation from bottom to top fibre of the girder as fatigue progressed. An increase of the instantaneous stiffness of link slab (Fig. 6c) of specimen B4H from 45.00 kN/mm to 60.07 kN/mm was observed during fatigue loading due to the flexibility of the RC deck girder, such that fatigue load caused deformation of bridge span rather than transferring to the link slab.

Figure 7a shows the variation of mid-span strains at the top and bottom fibre and in embedded rebar of ECC-LS during fatigue loading. Table 3 also summarizes strains at the start and end of fatigue cycles and associated strain bandwidth calculated as the difference between end and beginning of fatigue cycles. ECC tensile strain at the top fiber of link slab decreased by 10% at the end fatigue cycles possible due to location of cracks developed during testing. ECC compressive strain at the bottom fiber was increased

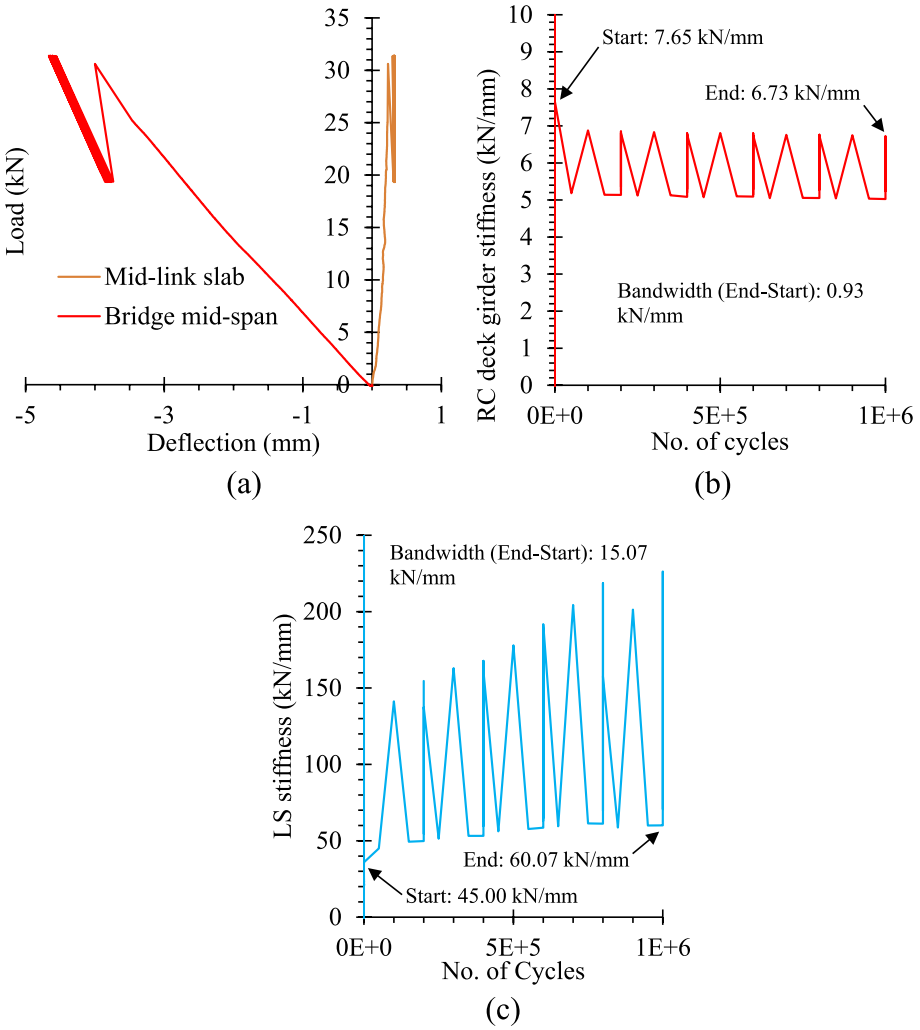

Fig. 6 RC deck girder joint-free bridge fatigue behaviour: **a** load-deflection response, (**b**) girder stiffness evolution, (**c**) link slab stiffness evolution

Table 3 Joint-free bridge link slab strains at beginning and end of fatigue cycles

Strain	Concrete Tensile Strain (microstrain)	Concrete Compressive Strain (microstrain)	Rebar Strain (microstrain)
At start of cycles	336	-338	523
At end of cycles	303	-532	3683 (>2000, yielded)
Bandwidth (End - Start)	-33	-194	3160

by 194 microstrain, however remained well within typical concrete crushing strain of -3500 microstrain throughout fatigue loading. Rebar tensile strain was increased by 3160 microstrain and yielded (exceeded 2000 microstrain) during fatigue cycles.

Figure 7b shows mid-span strain development in the bottom rebar of RC deck girder and top rebar of the link slab. The link slab rebar yielded during fatigue loading at cycle 271,728, however girder bottom reinforcement at mid-span remained within 1169

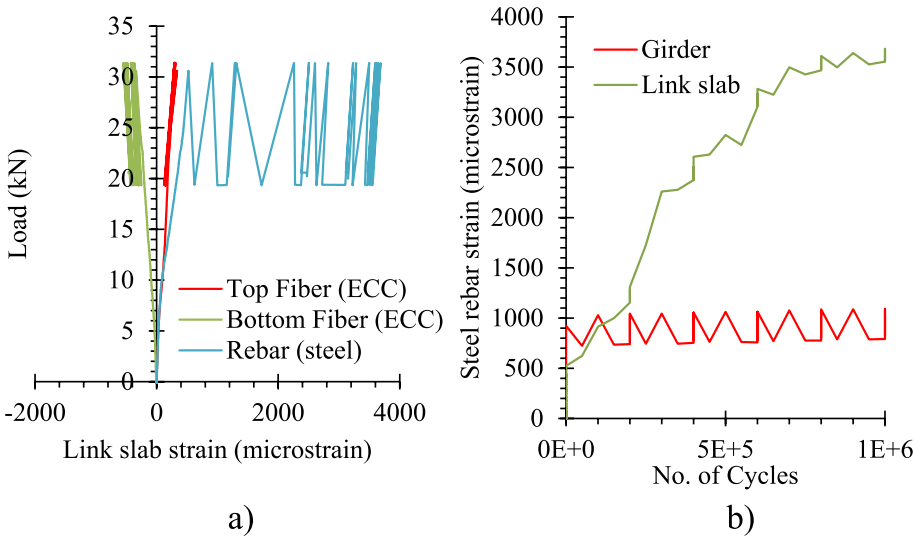

Fig. 7 Strain development in joint-free bridge during fatigue loading (**a**) link slab, (**b**) rebar strain in girder and link slab

Table 4 Strains in fatigued and non-fatigued bridges during post-fatigue loading to failure

Designation	Link slab mid-span strains at ultimate load (microstrain)			RC deck girder mid-span strains at ultimate load (microstrain)		
	ECC top surface (rs, total)	Steel rebar (rs, total)	ECC bottom surface (rs, total)	SCC deck top surface (rs, total)	Deck steel rebar (rs, total)	Girder bottom rebar (rs, total)
B0N	44	1480	-1003	-697 (n/a, n/a)	325 (n/a, n/a)	*2000 (n/a, n/a)
B4H	980 (46, 1026)	671 (3504, 4175)	-508 (-379, -887)	-1160 (-190, -1350)	600 (225, 825)	*2000 (269, 2269)

B0N Non-fatigued, *B4H* 40±10% fatigue stress level for 1,000,000 cycles, *rs* Residual strain at unloading to zero load, *total* total strain at ultimate load during post-fatigue loading, *n/a* Not applicable

*yielded (failure due to yielding of RC girder

microstrain (not yielded) after 1,000,000 cycles (Fig. 7b). This showed that the link slab failed during fatigue loading while the main RC deck girder remained intact.

4.3 Post-fatigue behaviour of RC joint-free bridge

After 1,000,000 fatigue cycles, the RC girder joint-free bridge B4H (at 40 ± 10% e stress level) was fully unloaded, then subjected to static load to failure. Post-fatigue behaviour in terms of deflection, rotation, energy dissipation and modes of failure were compared with those of virgin/non-fatigued companion specimen B0N. The results RC girder and companion steel girder with 7.9 times higher EI) bridge specimens (Chu et al. 2022a, 2023) subjected to same fatigue stress level and number of cycles were compared.

Figure 8(a-b) show the development of concrete/embedded rebar strain at mid-span in RC deck girder and ECC-LS for non-fatigued (B0N) and fatigued (B4H) specimens. Table 4 summarizes post-fatigue strains at ultimate load, post-fatigue residual strain at zero loading and total strain (residual strain + post fatigue strain). ECC and rebar strain development in fatigue-damaged RC girder or LS during post-fatigue monotonic loading was lower than their non-fatigued counterpart and these specimens exhibited lower post-fatigued failure load, as expected. The post-fatigue ECC tensile and compressive

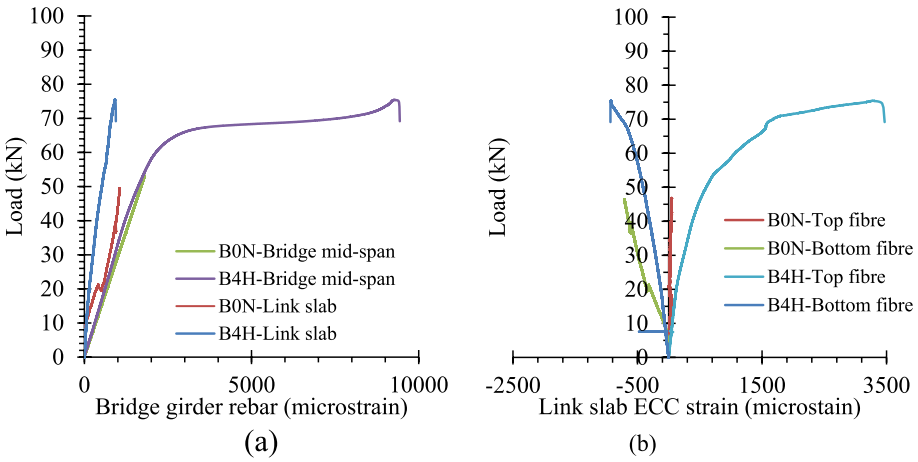

Fig. 8 **a** Rebar and (**b**) ECC strains (without residual for fatigued specimens) during post-fatigue loading to failure

strains (980 microstrain and −508 microstrain, respectively) remained also within the expected material limits (20,000 microstrain and 3500 microstrain, respectively) even after accounting for permanent set.

Figure 9(a-c) shows cracking and failure modes during fatigue loading and post-fatigue loading to failure of non-fatigued and fatigued bridge specimens. During fatigue loading of specimen B4H, flexural cracks were initiated from the top surface of the link slab and then from the bottom surface of RC girder near the mid-span regions as shown in Fig. 9a. It was noted that the link slab failed by rebar yielding during fatigue loading as confirmed from the strain exceeding 2000 micro strain at ultimate load (Table 3).

During monotonic loading both virgin (B0N) and fatigued (B4H) specimens, flexure cracks were developed near LS mid-span first followed by RC girder and extended and branched from the surface to the depth (Fig. 9b-c). In case of fatigued specimen, already developed flexural cracks in RC girder and link slab were extended and branched as load increased. ECC link slabs exhibited multiple micro-cracking behaviour with formation of distributed cracks in the debond zone. Both specimens, exhibited similar failure modes due to yielding of RC girder as can be seen from bottom rebar strains (exceeding 2000 micro-strain) at ultimate load of 63.05 kN and 58.09 kN, respectively (Table 4). As link slab in specimen B4N failed due to rebar yielding during fatigue cycles, RC girder was predominately carried the load during post-fatigue loading. Prior to failure, RC deck developed longitudinal cracking and also transverse cracking under the loading area when one of the flexure cracks propagated into a major crack (Fig. 9b-c). The average crack width in ECC-LS was 0.12 mm. The link slab rebar in the non-fatigued virgin specimen (B0N) did not yield even up to the end of the static test to failure with strain remaining less than 1500 microstrain as shown in Table 4. The failure observed in this study was in agreement with conventional concrete LS incorporated joint-free bridge documented in the literature (Caner and Zia 1998), where the bottom rebar of the RC deck girder was also the first component to yield. However, rebars in the conventional concrete link slab part of the joint-free bridge tested by Caner and Zia (1998) yielded shortly after the maximum

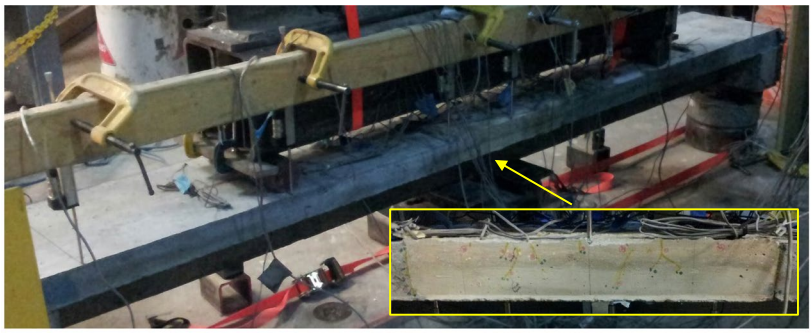

(a) Cracking of joint-free bridge (B4H) upon completion of fatigue loading

(b) Cracking and failure of non-fatigued joint-free bridge (B0N) after monotonic load to failure

(c) Failure of fatigued joint-free bridge (B4H) after monotonic load to failure

Fig. 9 Failure modes showing crack pattern of joint-free bridge specimens. **a** Cracking of joint-free bridge (B4H) upon completion of fatigue loading. **b** Cracking and failure of non-fatigued joint-free bridge (B0N) after monotonic load to failure. **c** Failure of fatigued joint-free bridge (B4H) after monotonic load to failure

load and exhibited only two cracks concentrated at the centre of the link slab with average width greater than 1.5 mm, rather than distributed across the debond zone as observed in this study where the link slab part was constructed using ECC. It is noted that the ECC link slab failed by rebar yielding during fatigue loading in specimen B4H, whereas it survived beyond the failure of the RC deck girder in the virgin specimen B0N.

Post-fatigued load-deflection (without residual strain) responses at mid span of RC deck girder and LS of fatigue damaged specimen B4H (monotonically loaded to failure) are compared with those of virgin specimen B0N in Fig. 10a with moment-rotation responses in Fig. 10b. The post-fatigue RC deck girder stiffness (10.9 kN/mm) of specimen B4H (calculated from Fig. 10a) was reduced by 14% compared to its pre-fatigue ramp stiffness (9.4 kN/mm) prior to start of fatigue loading (calculated from Fig. 6a) as shown in Table 5. Ultimate loads and associated deflections (including residual and cumulative deflections of fatigued specimen) of fatigued and virgin bridge specimens are presented in Table 5. The residual girder deflection of -1.40 mm at the end fatigue loading and cumulative deflection of -5.40 mm at ultimate load during post-fatigue loading also indicated fatigue-induced damage of specimen B4N. Post-fatigue ultimate load/strength of the fatigued damaged specimen B4N was reduced by approximately 5 kN besides stiffness compared to its non-fatigued B0N

Table 5 Summary of load, deflection, stiffness and energy absorbing capacities of bridges

RC Bridge	Ultimate load (kN)	RC girder mid-span deflection at ultimate load (rd, total) (mm)	Link slab mid-span deflection at ultimate load (rd, total) (mm)	RC deck girder stiffness (kN/mm)	Link slab stiffness (kN/mm)	Link slab energy absorbing capacity (J)
B0N	63.05	-4.53 (n/a, n/a)	2.24 (n/a, n/a)	-	-	24.2
B4H	58.09	-4.04 (-1.34, -5.40)	0.17 (0.14, 0.30)	10.9 (before), 9.4 (after)	112.5 (before), 118.3 (after)	1.5

B0N Non-fatigued, *B4H* 40±10% fatigue stress level for 1,000,000 cycles, *rd* Residual (non-recovered) deflection at unloading to zero load, *total* Total deflection at ultimate load during post-fatigue loading, *before* During ramp prior to start of fatigue loading, and *after* During post-fatigue monotonic load to failure, *n/a* Not applicable

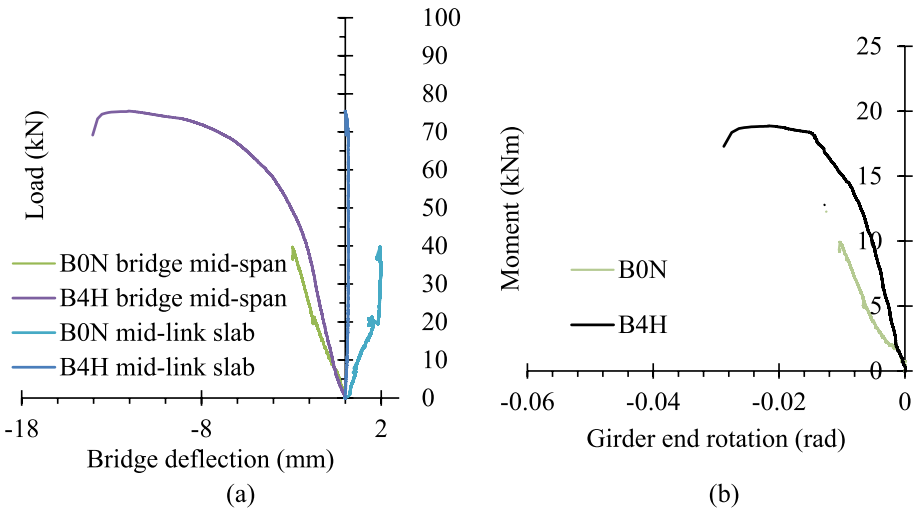

Fig. 10 Non-fatigued and fatigued joint-free bridge (**a**) load-deflection response, (**b**) moment rotation response

counterpart indicating damage during fatigue loading. In contrast, post-fatigue LS stiffness (slope of girder load-LS mid-span deflection response, Fig. 10a) of 118.3 kN/mm for specimen B4H was increased by 5% compared to pre-fatigue stiffness of 112.5 kN/mm as shown in Table 5. The LS stiffness increase could be attributed to the concentration of load and associated deflection in the RC deck girder rather than transferring to the link slab (which had already failed by rebar yielding during fatigue) as post-fatigue monotonic load increased.

Deflected shapes of pre and post-fatigued RC and composite steel (Chu et al. 2022a, 2023) girder bridges (based on cumulative deflection including residual deflection) during monotonic loading to failure are shown in Fig. 11 at 50% load level. Both RC and composite steel deck girder bridges exhibited typical behaviour of a joint-free bridge with positive and negative moment in the deck-girder spans and LS, respectively (as shown in Fig. 1). The inflection points in RC girder bridge in pre and post-fatigue stages were located at 12% and 10% of each span length, respectively (a reduction of 2% due to fatigue) which showed link slab damage resulting in decreased continuity. The pre and post-fatigue inflection points (11% and 9% of span, respectively showing a reduction of 2% due to fatigue) of composite steel girder bridge were less than their RC girder

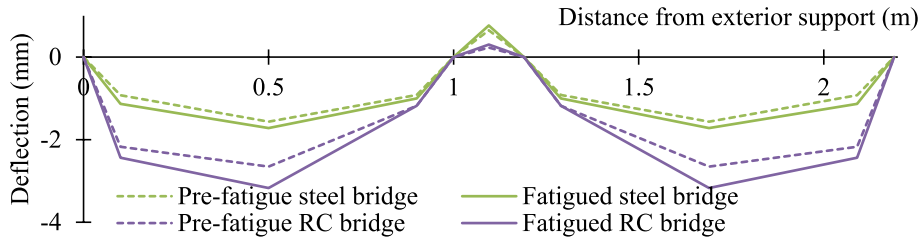

Fig. 11 Deflected shape of pre-fatigue and fatigued joint-free steel and concrete girder bridges at 50% load level

Table 6 Summary of load, moment and rotation capacities of fatigued/non-fatigued bridges

Designation	P_{LSy} (kN)	P_{all} (kN)	Ratio (P_{LSy}/P_{all})	θ_{ult} (rr, total) (rad)	Ratio (θ_{ult} /θ_{all})	M_{ult} (kNm)	$M_{r\text{-}g}$ (kNm) Eq. 1	Ratio (M_{ult}/$M_{r\text{-}g}$)
B0N	63.05	11.05	>5.71	-0.01494 (n/a, n/a)	3.98	15.76	15.85	1.02
B4H	24.09	11.22	2.15	-0.00896 (-0.00697, -0.01593)	2.39	14.52	15.85	0.94

B0N Non-fatigued, *B4H* 40±10% fatigue stress level for 1,000,000 cycles, θ_{ult} Girder end rotation at ultimate load, θ_{all} Maximum allowable girder end rotation of 0.00375 rad, M_{ult} Girder moment at ultimate load, $M_{r\text{-}g}$ Girder design moment as calculated by Equations 1 and 2, rr: residual rotation at unloading to zero load, total: Total rotation at ultimate load during post-fatigue loading, P_{LSy} Load when link slab rebar yielded, and P_{all} Load at θ_{all}, *n/a* Not apssplicable

counterpart. The link slab-to-girder EI ratio was far less for the steel bridge (0.09 compared to 0.69) so that it provides more flexibility for adjacent girders to behave effectively like a simply supported spans as desired in a joint-free bridge. In all cases, the inflection points were within the expected range (less than 25%) and slightly greater than 7.5% (assumed for LS specimen design). However, the bridge designer should take into account link slab-to-girder EI ratio in designing joint-free bridges to simulate effectively simply supported adjacent spans and control desired girder end rotation. Link slab-to-girder EI ratio is an important factor in controlling flexibility of adjacent girders and their end rotations in such bridges.

Link slab energy of the full bridge specimen was determined for comparison performance by taking area of the applied girder load -link slab deflection responses (Fig. 10a) up to yielding of girder bottom steel rebar. The RC girder bridge ECC link slab showed 93% post-fatigue energy reduction (reduced from 24.2 J to 1.5 J) compared with its virgin non-fatigued counterparts (Table 5). The same reduction percentage was also observed in RC and composite steel deck girder bridge counterpart which was reasonable as both failed by rebar yielding during fatigue cycles.

Figure 10b shows moment versus rotation curves of bridge specimens under o monotonic loading to failure. Fatigued damaged specimen B4H showed less moment and rotations at ultimate load compared to non-fatigued specimen B0N, as expected (Fig. 10b). Table 6 summarizes girder end rotation at ultimate load (Θ_{ult}), ratio of Θ_{ult} to maximum allowable rotation (Θ_{all}) of 0.00375 rad as per AASHTO (2015) (= $\Theta_{ult}/\Theta_{all}$, considered as a measure of the factor of safety for the RC deck girder), ratio of load at link slab rebar yielding (P_{LSy}) to load at Θ_{all} (P_{all}) (= P_{LSy}/P_{all} considered a measure of the factor of safety for the link slab), ultimate girder moment (M_{ult}), and ratio of M_{ult} to theoretical moment

($M_{r\text{-}g}$). The link slab rebar in the non-fatigued specimen B0N did not yield even after the RC deck girder failed. Therefore, P_{LSy} was greater than ultimate load of the specimen (63.05 kN) resulting in P_{LSy}/P_{all} of > 5.71. P_{all} was 11.05 kN which was almost 2.85 times lower than the service load of the bridge (31.5 kN). So link slab to girder EI ratio (particularly geometric and material properties) can be optimized to make the service load close to the P_{all} for economical design of the joint free bridges. Link slab of specimen B4H yielded (achieved its moment capacity of 2.01 kNm based on Eq. 3) approximately at 24.09 kN (P_{LSy}) with 0.01066 rad girder end rotation during fatigue loading resulted in a reduced P_{LSy}/P_{all} of 2.15 compared to 5.71 of the virgin specimen B0N. Despite significant reduction in P_{LSy}/P_{all}, the link slab of the fatigued bridge had the ability to undergo maximum allowable rotation of 0.00375 rad as per AASHTO (2015) and CSA (2006). In comparison, the steel girder bridge required 7.25 times the load to reach Θ_{all} compared to its concrete counterpart (Chu et al. 2022a, 2023). The Θ_{ult} values showed that both non-fatigued and fatigued RC deck girders were capable of achieving higher rotation than the maximum allowable Θ_{all}. Although the $\Theta_{ult}/\Theta_{all}$ (factor of safety) decreased from 3.98 to 2.39, the RC deck girder still maintained sufficient capacity despite failure of the link slab during fatigue cycles.

Theoretical girder moment capacity ($M_{r\text{-}g}$) of 15.40 kNm calculated based on theoretical Eq. 1 resulted in $M_{ult}/M_{r\text{-}g}$ of 1.02 for virgin specimen B0N. After 1,000,000 fatigue cycles, the experimental moment (B4H) reduced to 95% (14.52 kNm, Table 6) of the theoretical value as the calculations are only applicable for the non-fatigued RC deck girder.

5 Conclusions

Two span RC joint-free bridge specimens with ECC-LS were subjected to static monotonic loading to failure as well as subjected to 1,000,000 cycles of fatigue loading at 40 ± 10% stress level before being monotonically loaded to failure. Based on the experimental investigation, and in comparison, with results for dimensionally and materially similar composite steel deck girder incorporated The following conclusions were drawn from the study:

- During fatigue loading, the RC deck girder joint-free bridge with ECC-LS showed greater girder mid-span deflection increase, and higher stiffness degradation compared with its composite deck-steel I girder counterpart. In addition, ECC-LS exhibited distributed micro-cracking and failed due to steel yielding.
- ECC-LS in RC deck girder bridge exhibited 91% and 93% decrease in post-fatigue deflection and energy absorbing capacity at ultimate load compared with pre-fatigue values. Since the link slab rebar yielded during fatigue cycles, it's contribution to ultimate load capacity was limited during post-fatigue monotonic load to failure. The LS energy reduction was similar for RC and its counterpart steel-concrete composite girder incorporated joint-free bridge specimens.
- LS reinforcement yielded at 0.01066 rad girder end rotation during fatigue loading which suggested its capability to withstand maximum allowable rotation of 0.00375 rad. Both non-fatigued and fatigued RC deck girders were capable of achieving higher rotation than the maximum allowable and maintained sufficient capacity despite failure of the LS during fatigue cycles.

- The inflection points in RC joint-free bridge were within the expected range - slightly greater than 7.5% assumed for LS design. Theoretical equations are good in predicting non-fatigued RC deck girder moment capacity reasonably well with the ratio of experimental to predicted values of 1.02. Modification is needed to determine moment capacity of fatigued damaged specimens.
- The study confirms the viability of constructing RC deck girder join-free bridges with ECC-LS. However, designer should optimize LS-to-deck girder EI ratio to achieve desired girder end rotation and more investigation is needed.

Abbreviations

RC	Reinforced concrete
ECC	Engineered cementitious composite
SCC	Self-consolidating concrete
LS	Link slab
M_{r-g}	Moment capacity of RC girder
φ_s	Steel material reduction factor
f_y and A_s	Rebar yield strength and area, respectively
d	Effective section depth
a	Rectangular stress block depth
φ_c	Concrete material reduction factor
f'_c	Concrete compressive strength
b_e	Effective width of the slab
t_s	The total slab thickness
d_t	Distance from top surface to rebar centreline
y_t	Distance from top surface to neutral axis
y_b	Fistance from the neutral axis to bottom surface
f_{cr}	Cracking strength of ECC under uniaxial tension
f_c	Concrete compressive stress
M_{r-LS}	Moment capacity of link slab
E	Modulus of elasticity
I	2nd moment of area of girder
ϵ_y	Yield strain of steel

Acknowledgements
Sincere thanks to the technical staffs of the Structure and concrete laboratories of the Toronto Metropolitan University (TMU), Canada.

Authors' contributions
KMA Hossain: Conceptualization; Formal analysis, Funding acquisition, Investigation, Methodology, Project administration, Supervision, Writing – original draft, Writing – review & editing.
K Chu: Investigation, Formal analysis, Methodology, Writing – original draft, Writing – review & editing.
M Lachemi: Funding acquisition, Supervision, Writing – review & editing.

Funding
Authors acknowledge the financial support provided by the Natural Science and Engineering Research Council (NSERC) Canada.

Availability of data and materials
Presented in the main paper.

Declarations

Ethics approval and consent to participate
Not applicable.

Consent for publication
Not applicable.

Competing interests
No competing interests.

Received: 7 December 2023 Accepted: 2 January 2024
Published online: 03 February 2024

References

AASHTO (2015) AASHTO LRFD Bridge Design Specifications, 7th edn. AASHTO, Washington DC
Alampalli S, Yannotti AP (1998) In-service performance of integral bridges and joint less decks. Transp Res Rec 1624(98):1–7
Caner A, Zia P (1998) Behavior and design of link slabs for joint less bridge decks. PCI J 43:68–80
Chu K, Hossain KMA, Lachemi M (2021) Numerical Investigation on Static Behaviour of Steel- and GFRP-Reinforced ECC Link Slabs. Arabian J. of Science and Engineering, 2021, Springer, Issue 11, https://doi.org/10.1007/s13369-021-05644-1
Chu K, Hossain KMA, Lachemi M (2020) Fatigue behavior of GFRP-reinforced ECC link slabs under variable stress levels and number of cycles. Eng Struct 222:111130. https://doi.org/10.1016/j.engstruct.2020.111130
Chu K, Hossain KMA, Lachemi M (2022) Experimental and numerical study on joint-free bridges with steel or gfrp-reinforced ecc link slab subjected to static loading. Construct Build Mater 327(2022):127035. https://doi.org/10.1016/j.conbuildmat.2022.127035
Chu K, Hossain KMA, Lachemi M (2022) Static and fatigue behaviour of ECC link slabs in reinforced concrete girder joint-free bridges. Structures 41:1301–1310. https://doi.org/10.1016/j.istruc.2022.05.080
Chu K, Hossain KMA, Lachemi M (2023) Joint-free bridges with steel and GFRP-reinforced ECC link slabs under fatigue loading. Structures 47:814–828. https://doi.org/10.1016/j.istruc.2022.11.093
CSA (2006) Canadian highway bridge design code, CAN/CSA-S6-06. Canadian Standards Association, Mississauga
Hossain KMA, Attarde S, Anwar MS (2019) Finite element modelling of profiled steel deck composite slab system with engineered cementitious composite under monotonic loading. Eng Struct 186:13–25
Hossain KMA, Ghatrehsamani S, Anwar MS (2015) Flexural fatigue performance of ECC link slabs for bridge deck applications. In K. Mahmoud (Ed.), Sustainable Bridge Structures, Proceedings of the 8th New York City Bridge Conference. New York City: CRC Press. pp. 247–260
Hossain KMA, Hossain MA, Manzur T (2020) Performance of engineered cementitious composite covered or wrapped self-consolidating concrete beams under corrosion. Eng Struct 219:110801
Hossain KM, Parajuli S, Manzur S (2021) Axial Behaviour of columns confined with engineered cementitious composite, ACI Struct J. 119(1). https://doi.org/10.14359/51734217
Huang W, Gong F, Jin W, Maekawa K (2021) Numerical analysis of high and low-cycle flexural fatigue for reinforced concrete beams under full-range of varying amplitudes, structural concrete. J Fib 22(4):2167–2183. https://doi.org/10.1002/suco.202100074
Karim R, Shafei B (2021) Performance of fiber-reinforced concrete link slabs with embedded steel and GFRP rebars. Eng Struct 229:111590
Kim YY, Fischer G, Li VC (2004) Performance of bridge deck link slabs designed with ductile engineered cementitious composite. ACI Struct J 101(6):792–801
Lepech MD, Li VC (2009) Application of ECC for bridge deck link slabs. RILEM J Mater Struct 42(9):1185–1195
Li VC (2003) On Engineered Cementitious composites (ECC) - a review of the material and its applications. J Adv Concrete Technol 1(3):215–230
Li VC (2019) Mechanical properties of Engineered Cementitious composites (ECC). Engineered Cementitious composites (ECC). Springer Berlin Heidelberg, Berlin, Heidelberg, pp 101–137
Li VC, Fischer G, Kim Y, Lepech M, Qian S, Weimann M, Wang S (2003) Durable link slabs for jointless bridge decks based on strain-hardening cementitious composites. Michigan Department of Transportation research, Michigan DOT, Lansing
Li M, Li VC (2011) High-early-strength ECC for fast, durable concrete repair-material properties. ACI Mater J 108(1):3–12
Sahmaran M, Lachemi M, Hossain KMA, Li VC (2009) Influence of aggregate type and size on ductility and mechanical properties of engineered cementitious composites. ACI Mater J 106(3):308–316
Sherir MA, Hossain KMA, Lachemi M (2018) Permeation and transport properties of self-healed cementitious composite produced with MgO expansive agent. ASCE J of Mater Civil Eng 30(11):04018291. https://doi.org/10.1061/(ASCE)MT.1943-5533.0002466
Siad H, Lachemi M, Sahmaran M, Hossain KMA (2018) Advanced engineered cementitious composites with combined self-sensing and self-healing functionalities. Constr Build Mater 176:313–322
Yeganeh AE, Hossain KMA (2023) Structural behavior of shear deficient high performance reinforced concrete exterior joints under bending. Structures 48:1707–1721
Zhang Z, Zhang Q, Li VC (2019) Multiple-scale investigations on self-healing induced mechanical property recovery of ECC. Cem Concr Compos 103(May):293–302
Zhang L, Zheng Y, Yu Y, Hu S, Wu Z, Di B, Guo Y, Li M (2021) Structural performance evaluation of ECC link slabs reinforced with FRP bars for jointless bridge decks. Constr Build Mater 304:124462. https://doi.org/10.1016/j.conbuildmat.2021.124462
Zhou M, Shao Z, Hassanein MF (2021) Bending behaviour of reinforced concrete/engineered cementitious composite beams. Mag Concr Res 73(16):810–818. https://doi.org/10.1680/jmacr.19.00380

Publisher's Note

Springer Nature remains neutral with regard to jurisdictional claims in published maps and institutional affiliations.